



## Determination of U-bolt connection load capacities in overhead sign support structures

Zhengyu Liu<sup>a,\*</sup>, Brent M. Phares<sup>b</sup>

<sup>a</sup> Bridge Engineering Center, Iowa State University, Ames, IA 50010, USA

<sup>b</sup> Department of Civil, Environmental and Construction Engineering, Iowa State University, Ames, IA 50010, USA



### ARTICLE INFO

#### Article history:

Received 10 October 2019

Received in revised form 25 February 2020

Accepted 11 April 2020

Available online 24 April 2020

#### Keywords:

Finite element modeling

Highway sign trusses

Overhead sign supports

U-bolt load capacity

### ABSTRACT

The load capacities of the U-bolt connections used in steel overhead sign trusses for the Iowa Department of Transportation (DOT) are not known because the bolts are used in ways that do not match available manufacturer data. Although these U-bolt connections appear to have performed satisfactorily in the past, there has been a growing safety concern in recent years because of the need for overhead sign trusses to support larger signs with greater span lengths. The objective of this project is to develop effective and efficient methodologies to realistically estimate the capacity of the U-bolt connections specified in the actual Steel Overhead Sign Truss (SOST) design standards. To achieve this objective, a literature search on the utilization and modeling techniques for U-bolt connections was first conducted. Three laboratory tests were then performed on two types of specimens with loading directions of 0° and 90° for the Type-A specimen and 0° for the Type-B specimen. The data collected from the tests were used to calibrate finite element models (FEM). Finally, the calibrated models were then used in a parametric study to calculate the yield and ultimate capacity of both types of specimens with various material properties and load resultant directions.

© 2020 Elsevier Ltd. All rights reserved.

## 1. Introduction

The current Iowa DOT Steel Overhead Sign Truss (SOST) design standards utilize U-bolt connections to anchor a four-chord horizontal space truss to support columns at each end of the space truss. The SOST standards also utilize U-bolt connections to attach vertical sign-support members to the front-top and front-bottom chords of the space truss. The U-bolt was first developed for the use in the mechanical and vehicle industry and has been used for decades; its use in the infrastructure area is not very common. Although some manufacturers provide the tensile and shear capacities for the U-shape rod, the actual load capacities of the U-bolt connection (with the associated elements including pipe, saddle, base beam etc.) on the SOST has not been investigated yet.

The Current SOST U-bolt dimensional and material properties are substantially the same as those used in the earlier STEel OverHead (STOH) sign truss design standards, which were utilized from about 1970 to 2011. It is reassuring that these type of U-bolt connections appear to have performed satisfactorily for more than 40 years. However, there is a concern due to an ever-increasing need for the Iowa DOT's overhead sign trusses to support larger signs by trusses with even greater span lengths. It is possible that the actual design loads may already exceed (or may soon exceed) the capacities for the current type

of U-bolt connections. It is imperative to determine if the U-bolt connections have adequate strength to safely perform in current overhead sign support structures, as well as in future ones that will need to resist even greater loads. To ensure that these special trusses can safely support the required loads, it will be necessary to know if the U-bolt connections have sufficient strength.

A literature search indicated few research investigations on the capacity of U-bolt connection in civil engineering. However, related research was found in the fields of mechanical and vehicle engineering. Diamantoudis and Apostolopoulos [1] developed an FEM on a U-bolt system that was designed to secure a plate to a truck fame member. The objective of this research was to investigate the stress distribution on the U-bolt and C channel, and to determine whether the maximum stress exceeded a certain stress limitation. The results indicated that the maximum stress on the U-bolt occurs on the shank of the U-bolt, and the C channel experienced the highest bending stress at the bottom corner. Kirby and Charniga [5] created a FEM of a U-bolt system that used to clamp a leaf spring pack, axle seat, and lower bracket to the axle tube. The goal of the research was to address noise concerns by investigating the stresses in the leaf spring when it was subject to twisting. The analytical results were output and compared to the experimentally measured results on the axle seat. Shetty [8] investigated the load capacity and stress distribution on a suspension component in the onboard weighing system of off-highway log trucks. The suspension component of interest consisted of a trunnion saddle, a

\* Corresponding author.

E-mail addresses: zhengyu@iastate.edu (Z. Liu), bphares@iastate.edu (B.M. Phares).

U-bolt, and a leaf spring. During the research, laboratory tests were conducted to collect strain data from the suspension components of the off-highway log tractor. The suspension system specimen was installed into a log truck and loaded with the weight of a slip-on water tank. A FEM was developed to determine the locations on the U-bolt surface that would provide the largest strain. The results indicated that the top of the curved portion of the U-bolt showed the maximum strain and was recommended as a preferred position for a future monitoring project.

It was found that the finite element method is the most common approach utilized (typically in combination with laboratory tests) to study the stress distribution on U-bolt assemblies of interest. However, different modeling approaches were adopted by the various researchers with the consideration of differences in their research objectives, efficiency in computation time, and model size capacity of the computer, etc. For example, in the models developed by Diamantoudis and Apostolopoulos [1] and Kirby and Charniga [5], the U-bolt shank and curve were modeled using a two-dimensional (2D) beam element, and the other components were modeled using a three-dimensional (3D) solid element. However, Shetty [8] created the whole U-bolt assembly using only 3D quadratic tetrahedral solid elements. On the model developed by Shetty [8] the contact behaviors between the U-bolt and leaf spring block, and between the leaf spring block and trunnion saddle were modeled using surface-to-surface contact elements. The preload due to the fastening torque was simulated by assigning an appropriate coefficient of thermal expansion and specifying a temperature change on the shank of the U-bolt.

Although research conducted on U-bolt connections is sparse, studies on normal steel bolts are quite abundant. The modeling technique commonly used for normal bolts can provide valuable reference to the finite element modeling of the U-bolt connection. For example, McCarthy and McCarthy [6] and McCarthy et al. [7] developed 3D FEMs to study the effects of bolt-hole clearance on the mechanical behavior of bolted composite joints. Nonlinear FEMs consisting of the bolt, two plates, a nut, and washers were developed on a single-bolt, single-lap connection to evaluate the modeling techniques. The analytical results were compared against experimental results to

determine the various parameters of the material properties and the contact mechanism. The preload was applied by assigning an orthotropic thermal expansion coefficient to the washer (allowing the thermal expansion/contraction only in the direction parallel to the longitudinal axial of bolt) and applying a positive temperature change onto the washer. Ju et al. [3] created a 3D elasto-plastic FEM to study the structural behavior of a butt-type steel bolted joint. Both bearing-type and slip-critical type connections were modeled using 3D solid elements for the bolt and plate. Contact elements were used to model the interface. The boundary conditions and locations of the contact elements. To account for the shear force being transferred from the plate directly to the bolt, a contact element was assigned at the vertical interface between the bolt and the plate. The preload was modeled by applying an initial displacement at the end of U-bolt shanks. Kim et al. [4] performed finite element analysis on a large marine diesel engine utilizing ANSYS software. To determine the best modeling technique for the bolted joint structure, four types of joint models, including a solid bolt model, a coupled model, a spider bolt model, and a no-bolt model, were developed and evaluated. The preload due to the fastening torque was modeled using thermal strain, and a surface-to-surface contact element was used at the interface between the head/nut and the flanges. The results indicated that the solid bolt model, which meshes the U-bolt shank and curve with the 3D solid element, provided the most accurate stress distribution on the U-bolt when compared with the experimental results.

Based on the results of the literature review, it was found that developing a FEM associated and calibrated with laboratory tests is the most commonly used approach to study the behavior of bolt-joined connections. The determination of the element type is a matter of computation time and computer capacity as related to model size. If enough computer time is available, the model with the solid element and surface contact element was found to provide the most accurate results. It was also found that model accuracy is sensitive to the definition of the contact behavior. It is essential to correctly model the contact interaction. Many approaches could be used to assign the preload (created by torque) to the FEM, including applying thermal strain on the shank or

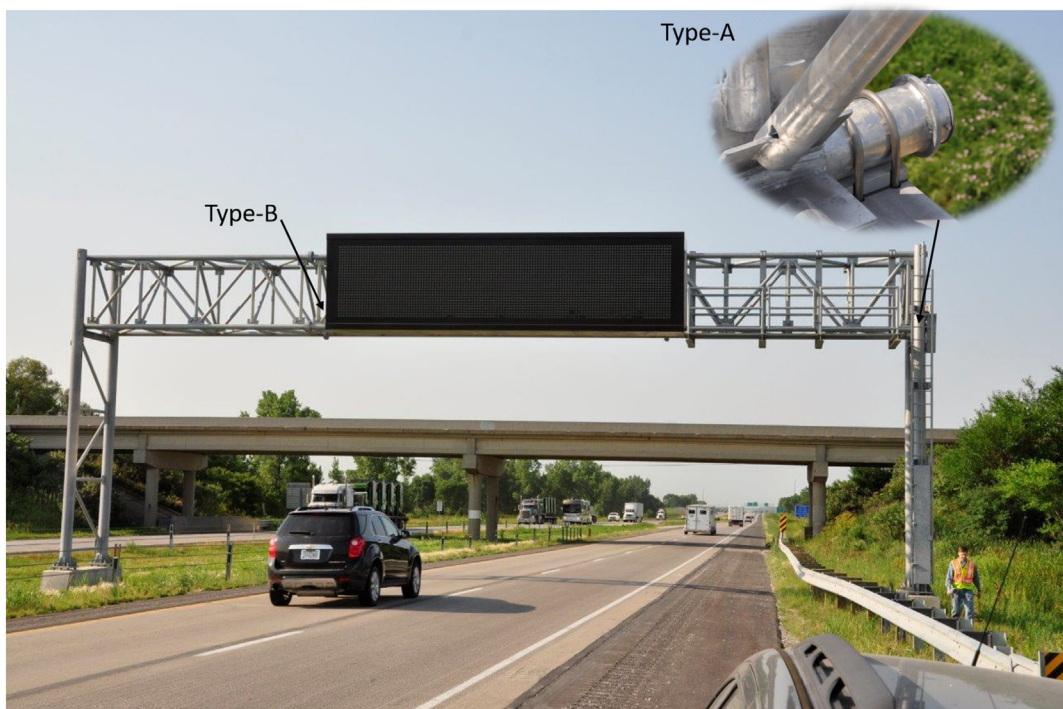


**Fig. 1.** U-bolt connections in the steel overhead sign truss.

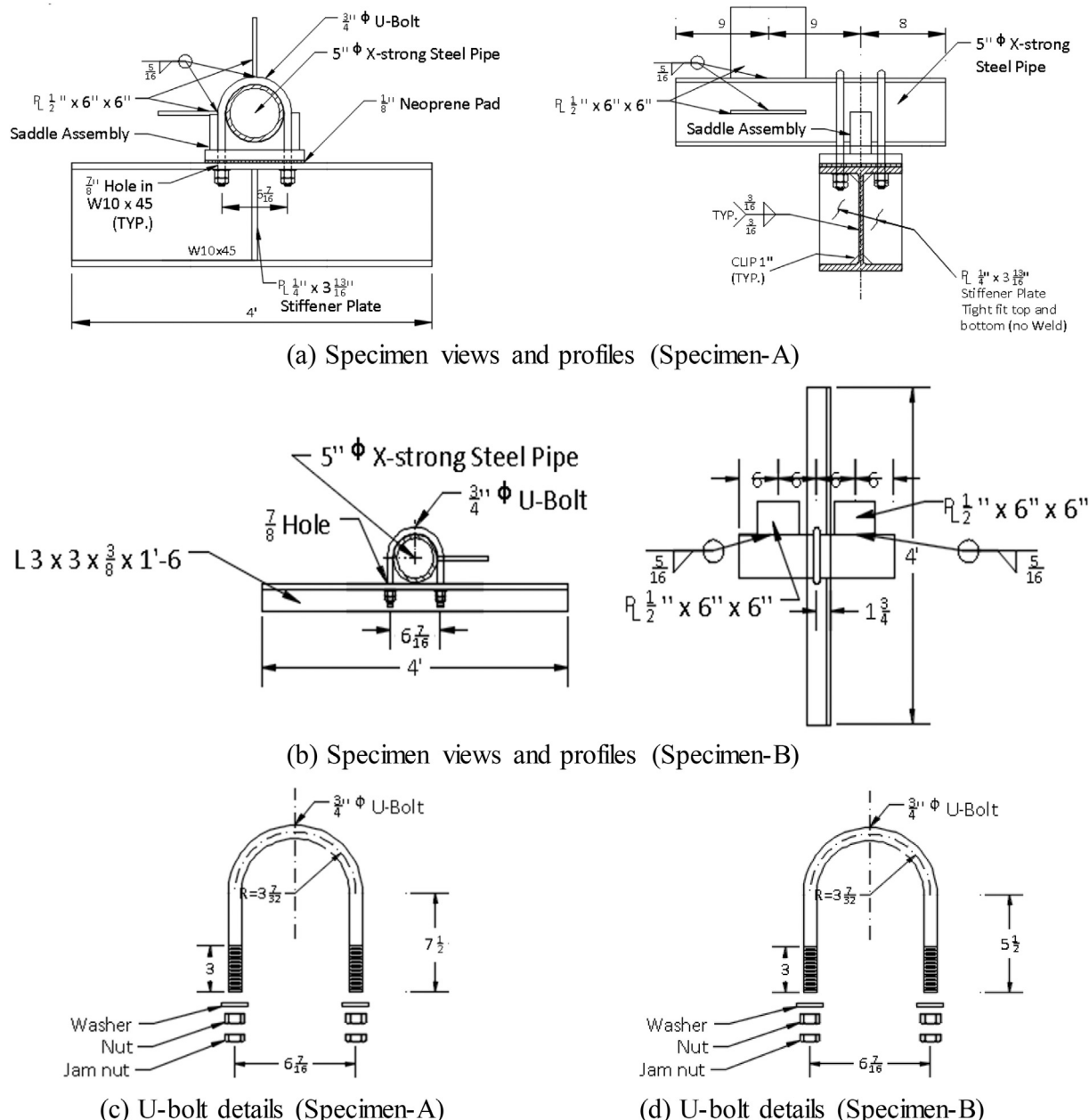


Fig. 2. Type-A U-bolt specimen design.

**Table 1**  
Nominal material types for laboratory tested specimen.

Part	Steel Grade <sup>a</sup>	Yield Strength (ksi)	Ultimate Strength (ksi)	Initial Young's Modulus (ksi)
U-bolt	A36	36	65	29,000
Pipe	A53-B	35	60	29,000
Saddle	A572-50	50	65	29,000
Load plate	A36	36	65	29,000
W-shaped beam	A992	50	65	29,000
Angle	A36	36	65	29,000

<sup>a</sup> Although multiple types of steel with different yield and ultimate strength are being used for the U-bolt on actual SOST designs in Iowa, the tests used A36 steel for the experimental study and calibration of the FEM. The performance of other types of steel were evaluated during the analytical parametric study.

washers, or assigning an initial displacement onto the bottom of the bolt.

The objective of this project was to develop methodologies and/or guidance on how to estimate the capacity of the U-bolt connections specified in the SOST design standards. To achieve the goal, an experimental program was conducted to load test U-bolt connections of the same dimensional and material properties used in the actual SOST design standards. A numerical modeling program was developed to assist in understanding the actual behaviors and failure modes of the U-bolt connections; these numerical models were validated against the load test data. Based on the experimental and numerical results, interaction diagrams were developed for the purpose of estimating the capacities of the U-bolt connections.

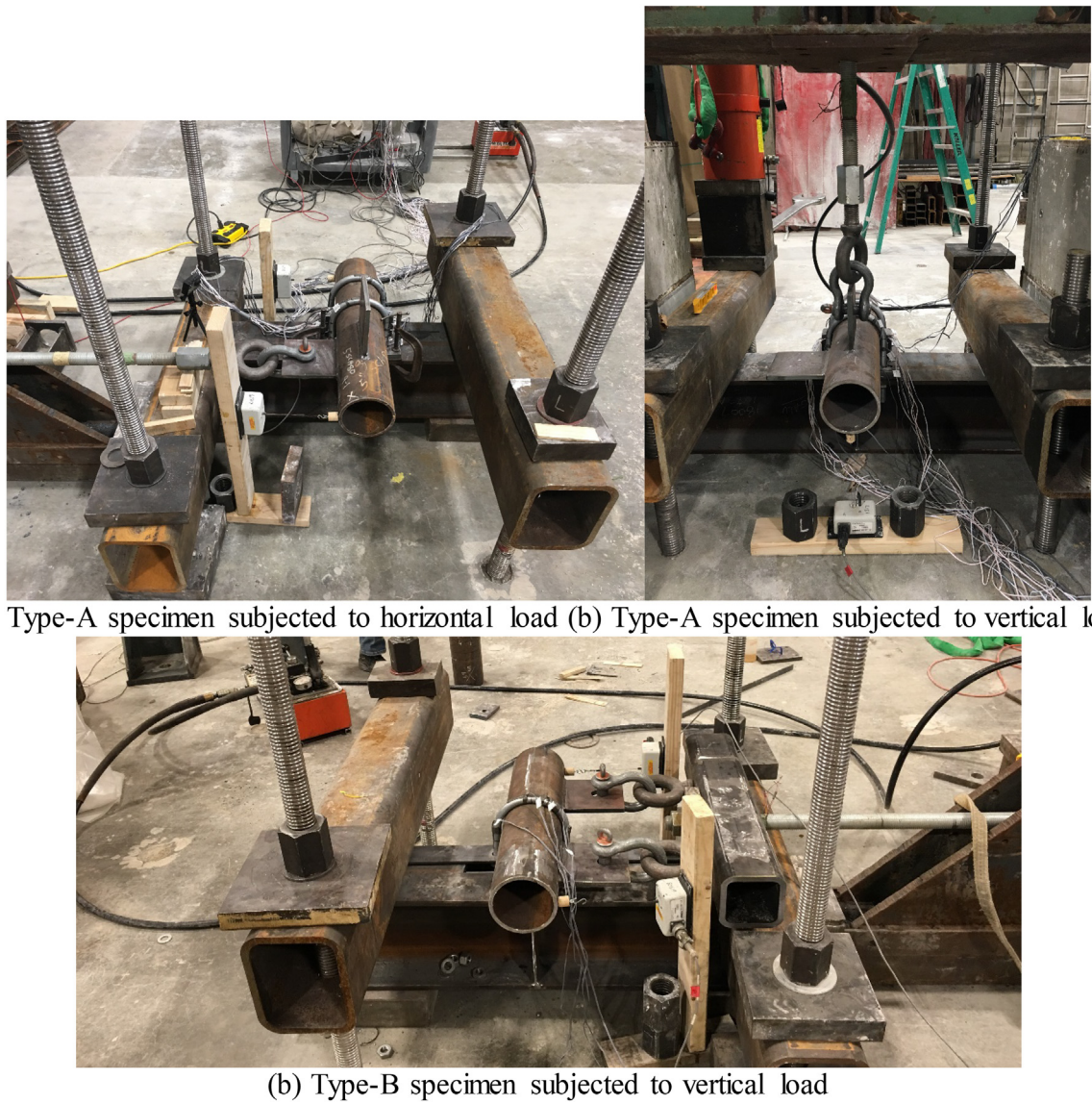


**Fig. 3.** Specimen setup before testing.

## 2. Laboratory investigation

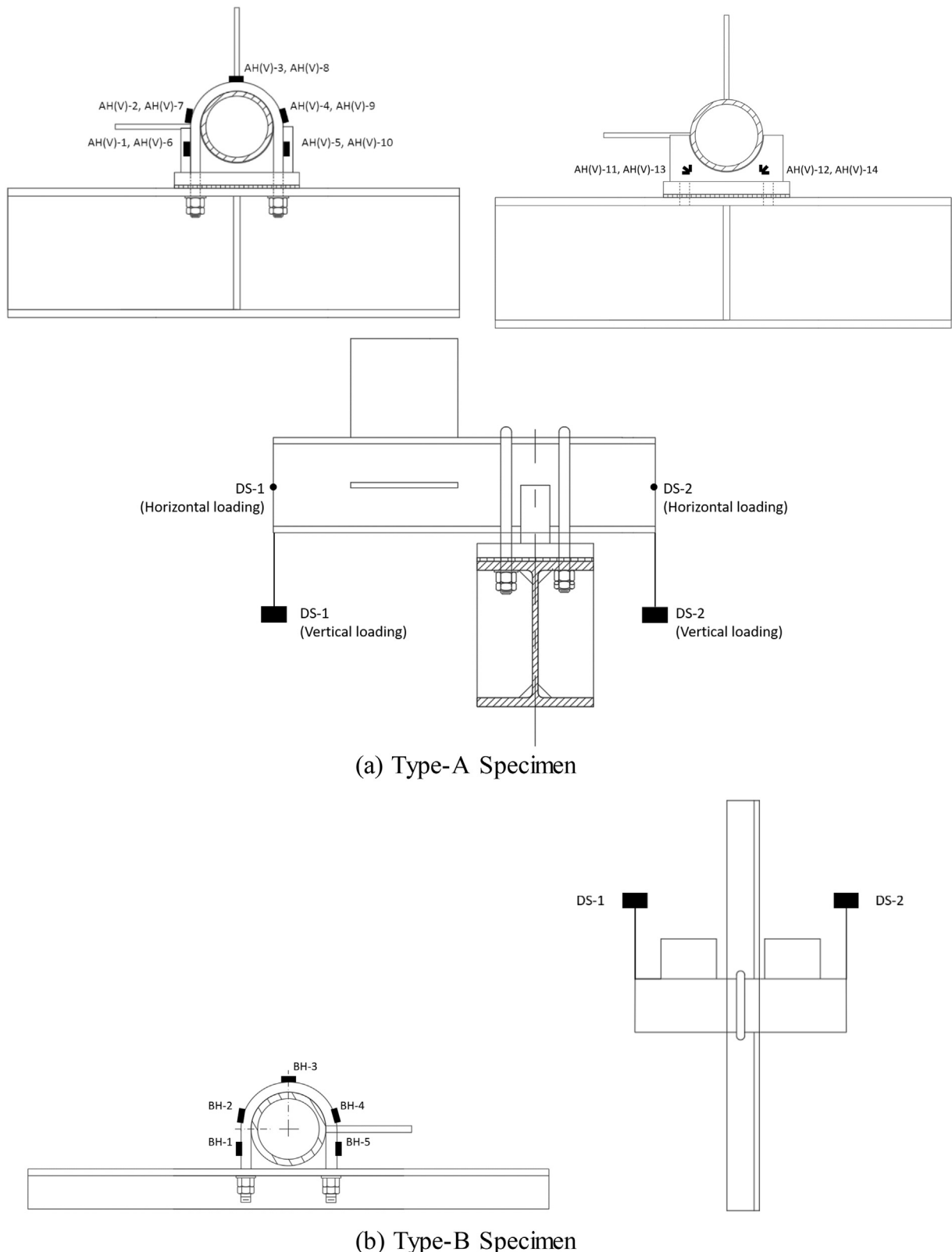
The objective of the laboratory testing was to monitor the structural behavior of the U-bolt, capture the failure mode when the bolt is subject to loading in different directions, and provide data for the calibration of the FEM. Two types of critical U-bolt connections were identified and selected for experimental evaluation (see Fig. 1 for the U-bolt locations in the SOST): the Type-A U-bolt connection used to anchor the bottom chords of the horizontal space truss to supporting columns at each end of the space truss and the Type-B U-bolt connection used to attach vertical sign support members to the front-top and front-bottom chords of the space truss. To simulate the critical load conditions applied on the two types of connections, two Type-A U-bolt connection specimens and one Type-B U-bolt connection specimen were fabricated, instrumented, and tested.

### 2.1. Type-A specimen

The specimens were designed with the material and geometric properties used in the actual SOST design standards. As shown in Fig. 2-a, the Type-A specimens consisted of a W-shaped steel beam, a

saddle assembly, a steel pipe with two steel plates, and the U-bolt components. The material designation and properties for each component are shown in Table 1. Two Type-A connection specimens were fabricated and tested. One of the Type-A connection specimens was loaded in the horizontal direction as shown in Fig. 3-a, and the other one was loaded in the vertical direction as shown in Fig. 3-b. The loads were applied on the plates welded to the pipe to simulate the loading mechanism in actual field installations. Before the application of the horizontal and vertical loads, a preload was applied by fastening the U-bolt utilizing a 1-ft long (approximate) wrench with the full effort of a human. The full effort of this person was tested using a net loading cell and resulted in about 30 lbf. The total torque applied on each shank was about 30 lbf-ft.

For both tests on the Type-A specimens, the instrumentation plan was the same, as shown in Fig. 4. Ten uniaxial foil strain gages and four rosette gages were installed on each specimen. To measure the strain change along the axis of the U-bolt, five uniaxial foil gages were installed on each U-bolt (shown in Fig. 4-a) with three at the curved part and two on the shanks at about 1.5 in. above the top surface of the saddle. The four rosette gages were installed at the sides of the saddle to measure the strain on the surface in multiple directions. In

**Fig. 4.** Instrumentation.

addition, two displacement transducers were used to measure the displacement change as shown in Fig. 4-c. The displacement transducers were placed at the two ends of the pipe and were used to measure the displacement change in the loading directions. The labels were

designated so that, A and B denote specimen type, H and V denote the loading direction in horizontal and vertical directions, respectively, and DS denotes the displacement transducers. On the Type-A specimen, AH-1 to AH-10 and AV-1 to AV-10 are the straight foil strain gage

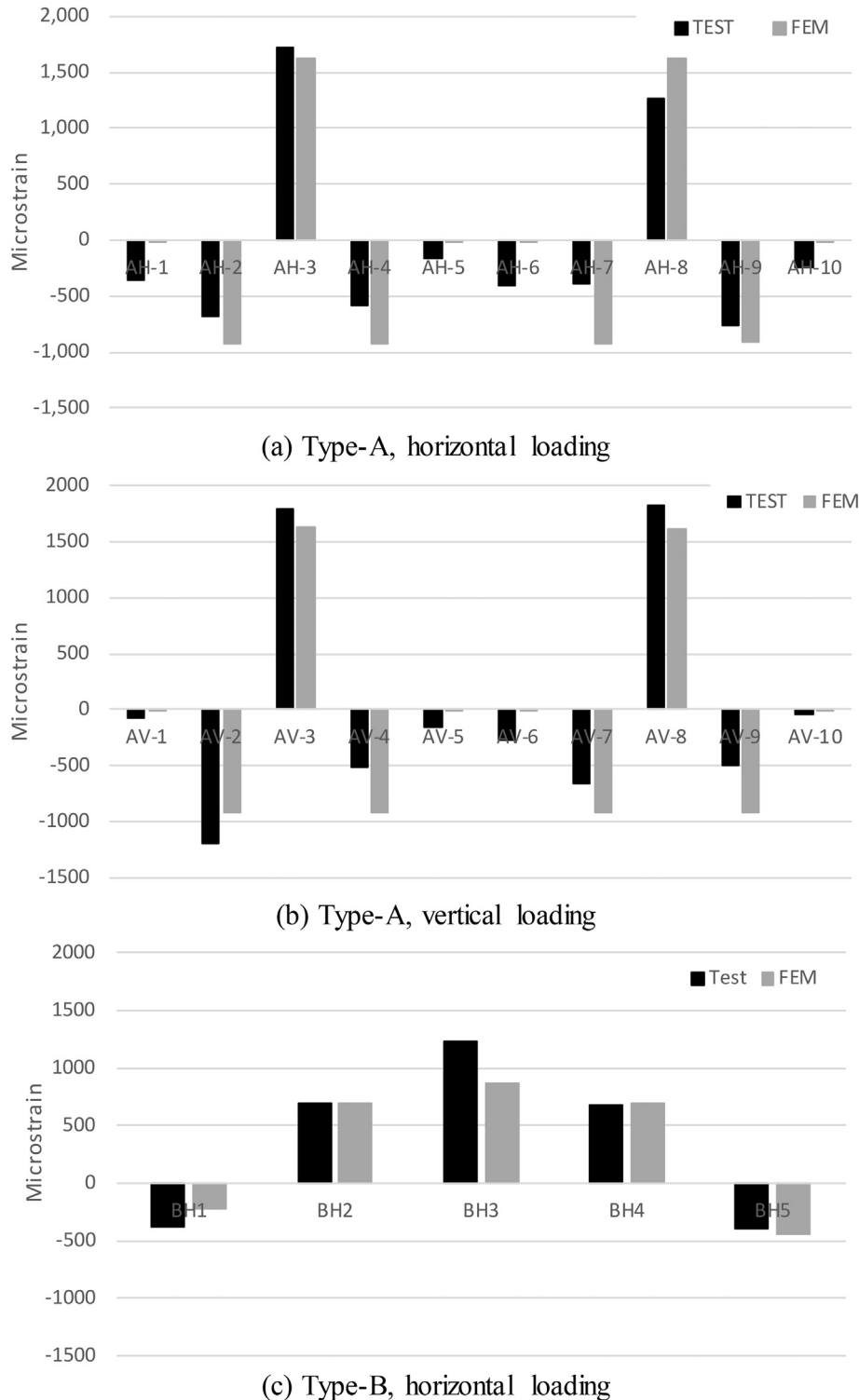
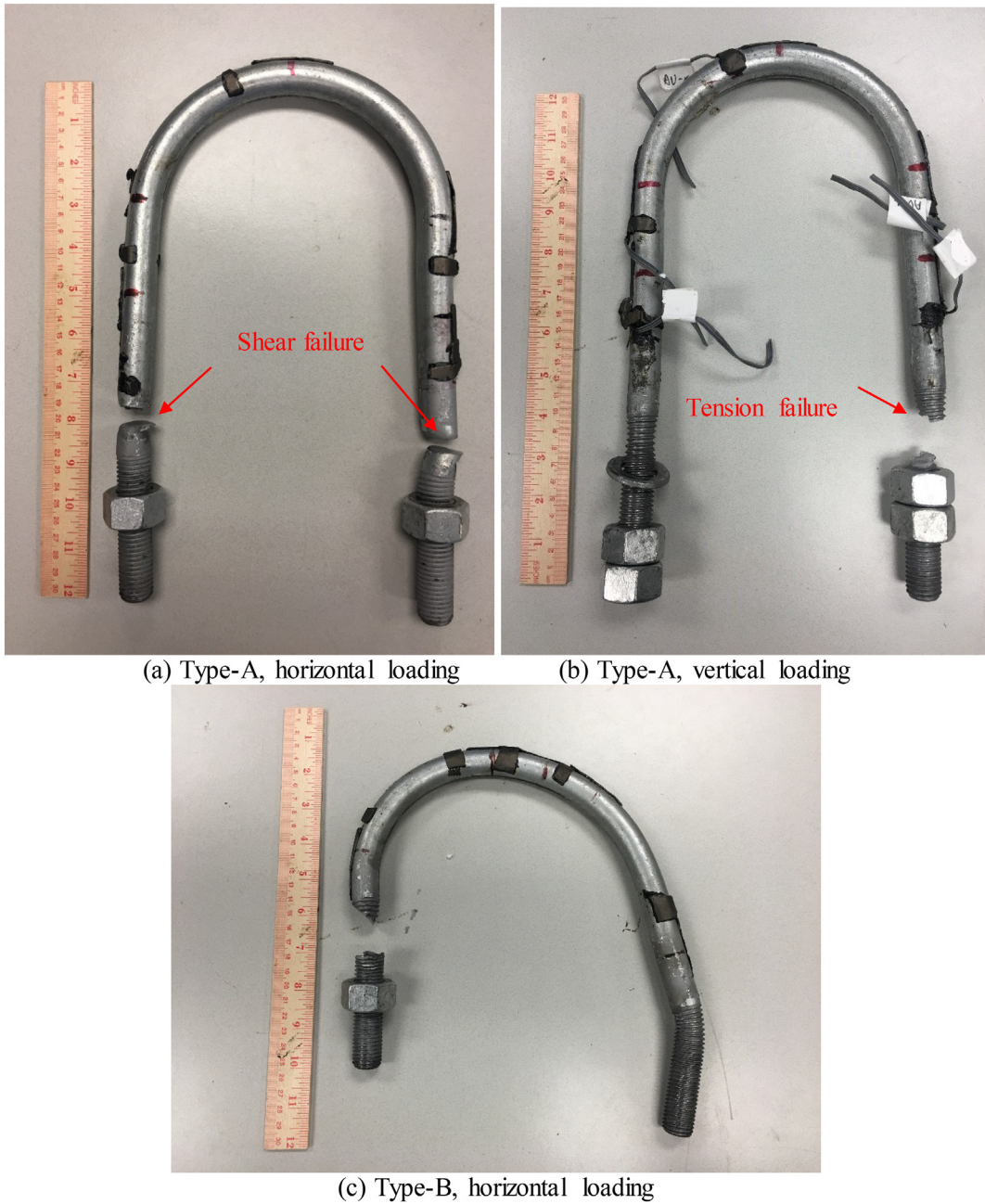


Fig. 5. Model validation by U-bolt strain due to preload.

attached on the U-bolt. The four rosette strain gages were designated from AH-11 to AH-14, and AV-11 to AV-14.

During the application of the preload, the strain change on the U-bolt was measured using the uniaxial foil strain gages attached along the axis of the U-bolt. Fig. 5-a shows the strain induced by the preload for the first Type-A specimen. The strain gages AH-3 and AH-8 attached on the top of the U-bolt captured the maximum strain in tension at about 1,250 to 1,750 microstrain. The other gages showed strain in

compression due to the bending effect. The specimen was then loaded subject to the horizontal load until failure with an ultimate capacity of 36 kips. The specimen broke in a shear-type failure of the U-bolt shanks (on the loading side) induced by the relative displacement between the saddle and the top flange of the W-shaped beam (see Fig. 6-a). Fig. 7-a shows the force vs. displacement curves from the testing. Due to the short extension length of the stringer in DS-1, the data beyond 30 kips was not able to be captured from DS-1. DS-2 kept functioning until



**Fig. 6.** Shear failure on the U-bolt shanks.

the end of the test. Fig. 8-a and -b shows the strain change along the axis of the U-bolt versus the applied load. Fig. 9 shows the strain data measured from the rosette gages (AH-11 and AH-14) attached on the sides of the saddle. The strains from the other rosette gages are small (less than 100 microstrain) even at the ultimate loading stage and are not presented.

The second Type-A specimen was preloaded following the same approach used on the first Type-A specimen and then loaded in the vertical direction. Fig. 5-b shows the strain change on the U-bolt induced by the preload. The data shows similar behaviors as those shown in Fig. 5-a and that the strains on the top of the curved part are in tension with a maximum magnitude of about 1,750 microstrain, while the others are in compression. The U-bolt broke with a tension failure at a thin cross-section (with a design diameter of 0.63 in. and a cross-sectional area

of  $0.31 \text{ in}^2$ ) in the thread region when the loading was 24 kips (see Fig. 6-b for the failure mode). Fig. 7-b shows the load versus displacement data. The strains from the rosette gages attached on the side of the saddle are small and not presented. Fig. 8-c shows the strain results in the first 5 kips that measured by the strain gage attached on the failed U-bolt. It was found that at the low load level, the strain gage attached at the top of U-bolt (AV-3) experienced a large strain first, although the final failure occurred at the shank near the thread region.

## 2.2. Type-B specimen

As shown in Fig. 2, the Type-B specimen consisted of an angle, a steel pipe, two steel plates, and the U-bolt components. The material type for each component was shown previously in Table 1. The angle was

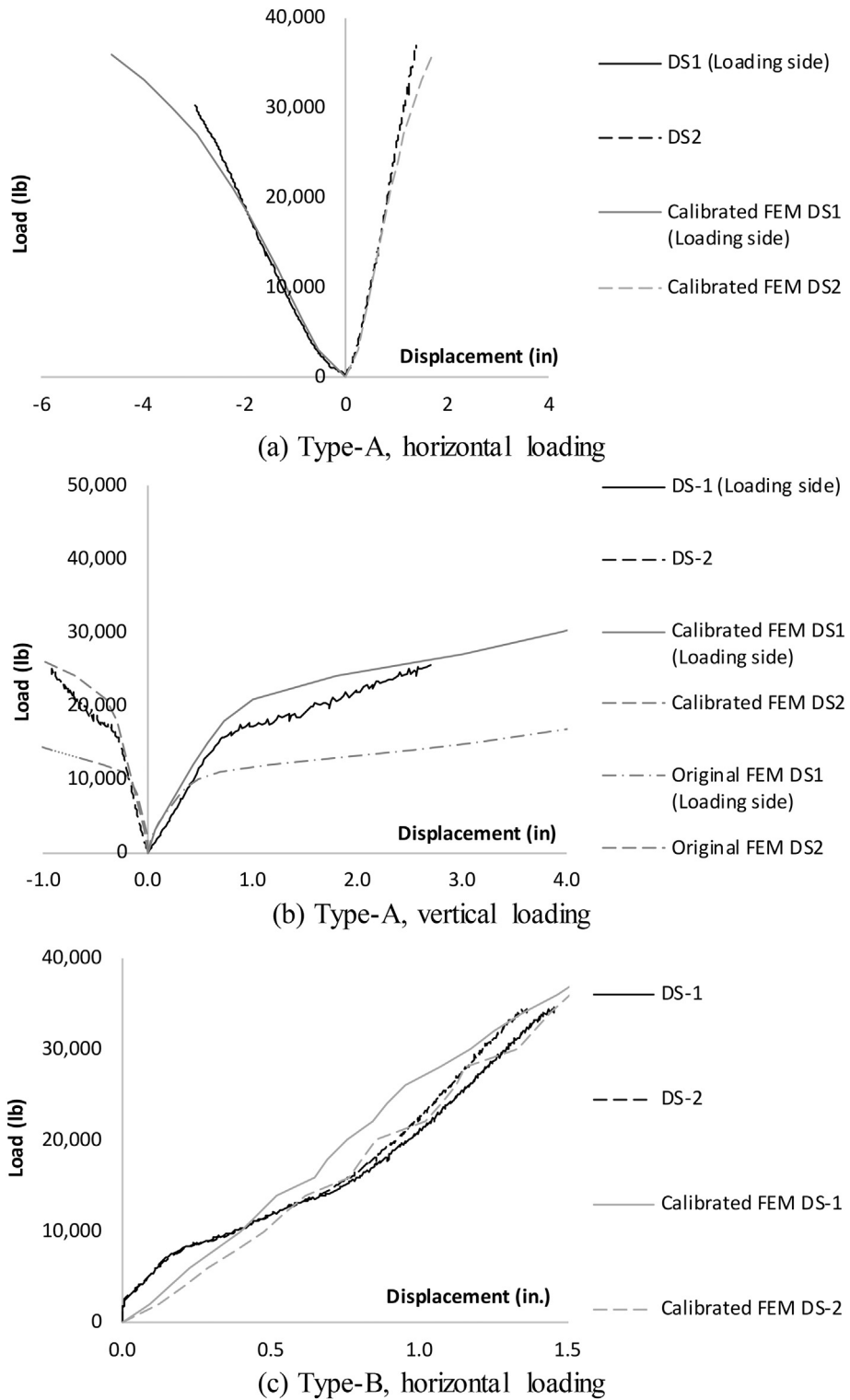


Fig. 7. Model validation by load vs. displacement curves.

fabricated using A36 steel and the other components were manufactured utilizing the same materials as those used for the Type-A specimen. The Type-B specimen was first loaded with the preload in the same way as the Type-A specimens, and then loaded with the horizontal load as shown in Fig. 3. The horizontal load was evenly applied on the two plates simultaneously. Fig. 4-b shows the instrumentation plan on the Type-B specimen. Five uniaxial foil strain gages were attached along the axis of the U-bolt on the exterior side and two displacement

transducers were used to measure the displacement in the horizontal direction. Fig. 5-c shows the strain measured on the U-bolt induced by the preload. Similar to the Type-A specimens, the maximum strain occurred at the top of the curved part of the U-bolt with a magnitude of about 1,250 microstrain. Subject to the horizontal load, the U-bolt on the Type-B specimen failed in the threaded region on the front leg (near the loading plate) with a shear failure as shown in Fig. 6-c. The total ultimate load carried by the specimen was about 35 kips. Fig. 7-c

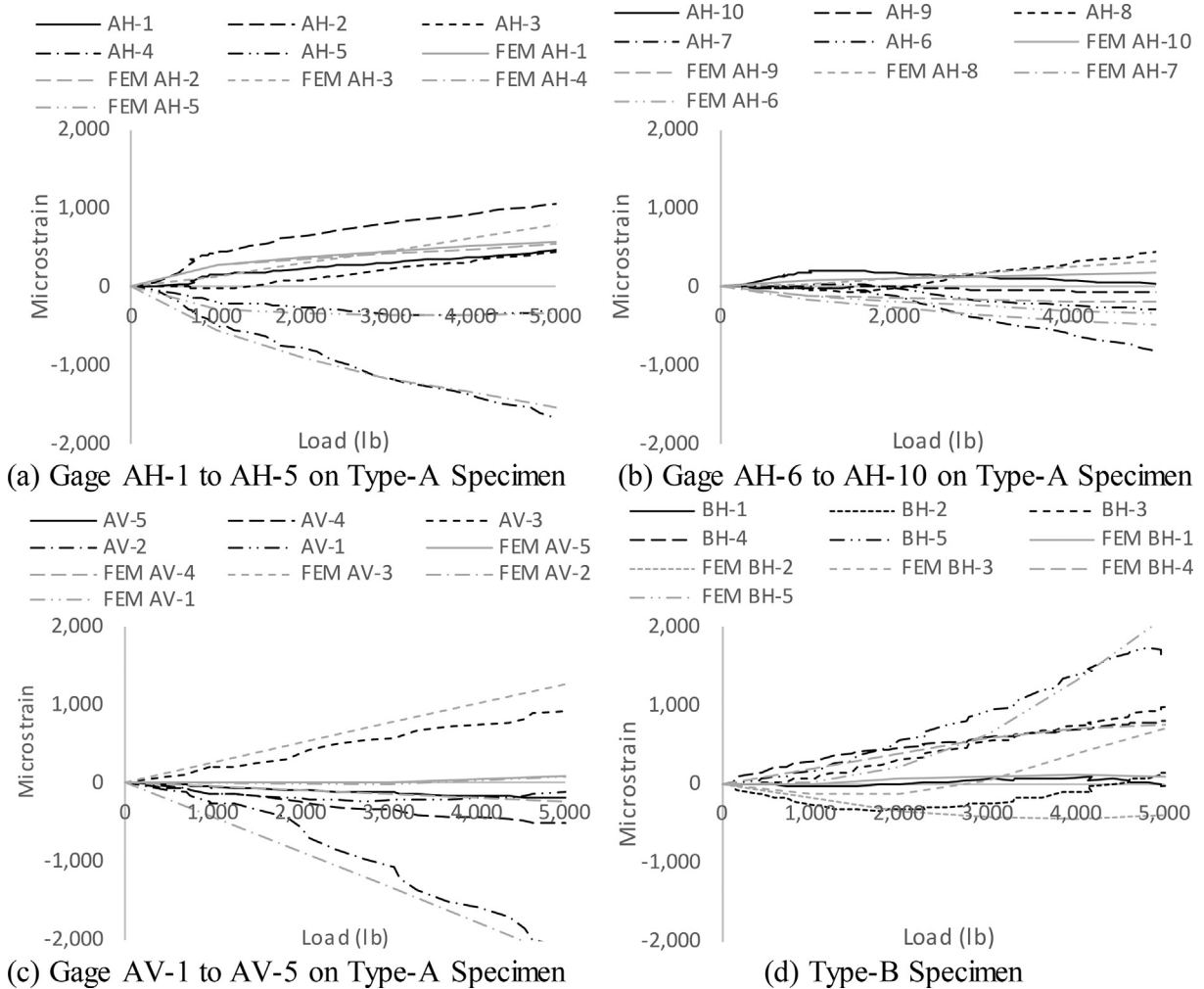


Fig. 8. Model validation by U-bolt strain.

shows load versus displacement curves for the Type-B specimen subject to the load. It can be seen that, before the load reached 18 kips, the specimen was loaded symmetrically, but, after that, a small difference in the displacement between the two ends of the pipe appeared. Fig. 8-d

shows the strain change for the first 5 kips on the U-bolt versus the loading. It was found that BH-5 attached at the front shank near the failure region always experience a higher tensile strain than the other strain gages.

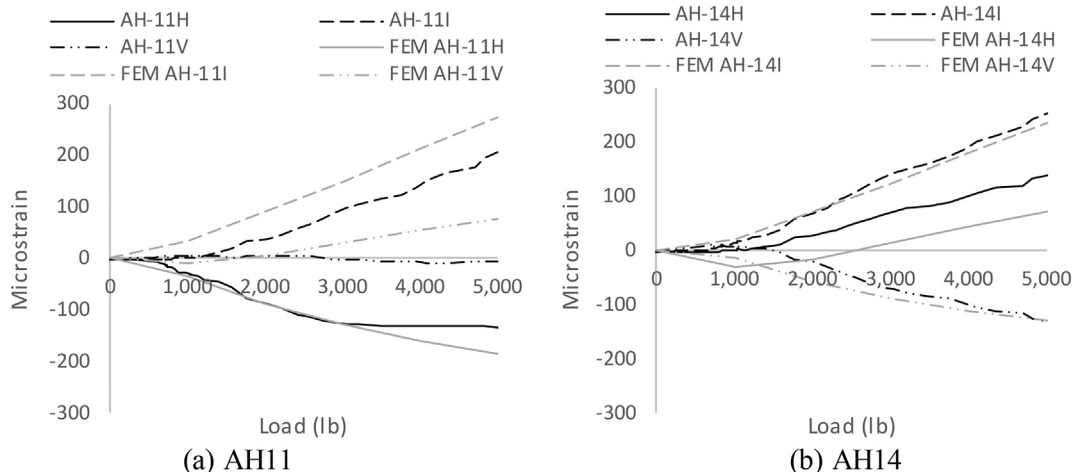


Fig. 9. Model validation by strain from rosette strain gage.

**Table 2**  
FEM details.

	Steel Grade	Element Type	Yield Strength (ksi)	Ultimate Strength (ksi)	Initial Young's Modulus (ksi)	Specimen Type
U-bolt	A36	Solid185	36	65	29,000	Type-A & -B
Pipe	A53-B	Solid185	35	60	29,000	Type-A & -B
Saddle	A572-50	Solid185	50	65	29,000	Type-A
Load plate	A36	Solid185	36	65	29,000	Type-A & -B
W-shaped beam	A992	Solid185	50	65	29,000	Type-A
Angle	A36	Solid185	36	65	29,000	Type-B
U-bolt (calibrated)	A36	Solid185	60	100	29,000	Type-A & -B
Pipe/U-bolt interface		Surface Contact Element				Type-A & -B
Saddle/pipe interface		Surface Contact Element				Type-A
Pipe/angle interface		Surface Contact Element				Type-B
Saddle/beam interface		Surface Contact Element				Type-A
Nuts and beam interface		Surface Contact Element				Type-A & -B
Shank and side of saddle and top flange of beam		Surface Contact Element				Type-A & -B

### 3. Model development and validation

To further interpret the test results and provide a valid analytical tool for the parametric study, FEMs were developed for the specimens. The results from the FEMs were compared against the test results to validate the modeling approach. A 3D nonlinear FEM was developed using the commercially available software ANSYS. All steel parts were modeled using Solid185 elements. Table 2 lists the material properties for each component. Since the FEM is a highly nonlinear model with large deformation, the true stress-strain curve, which was converted based on the engineering stress-strain relation, was input into the model. The engineering stress and strain that were in the engineering

software application neglect the necking effect, were established with an initial Young's modulus of 29,000 ksi and a peak strength strain of 0.2 for each component. The true stress and strain, which consider the necking effect, were calculated using Eqs. (1) and (2).

$$\varepsilon_{true} = \ln(1 + \varepsilon_{engineering}) \quad (1)$$

$$\sigma_{true} = \sigma_{engineering} \times (1 + \varepsilon_{engineering}) \quad (2)$$

where,  $\varepsilon_{true}$  is the true strain;  $\varepsilon_{engineering}$  is the engineering strain;  $\sigma_{true}$  is the true stress and  $\sigma_{engineering}$  is the engineering stress. Fig. 10-a shows both engineering and true stress-strain curves for each component.

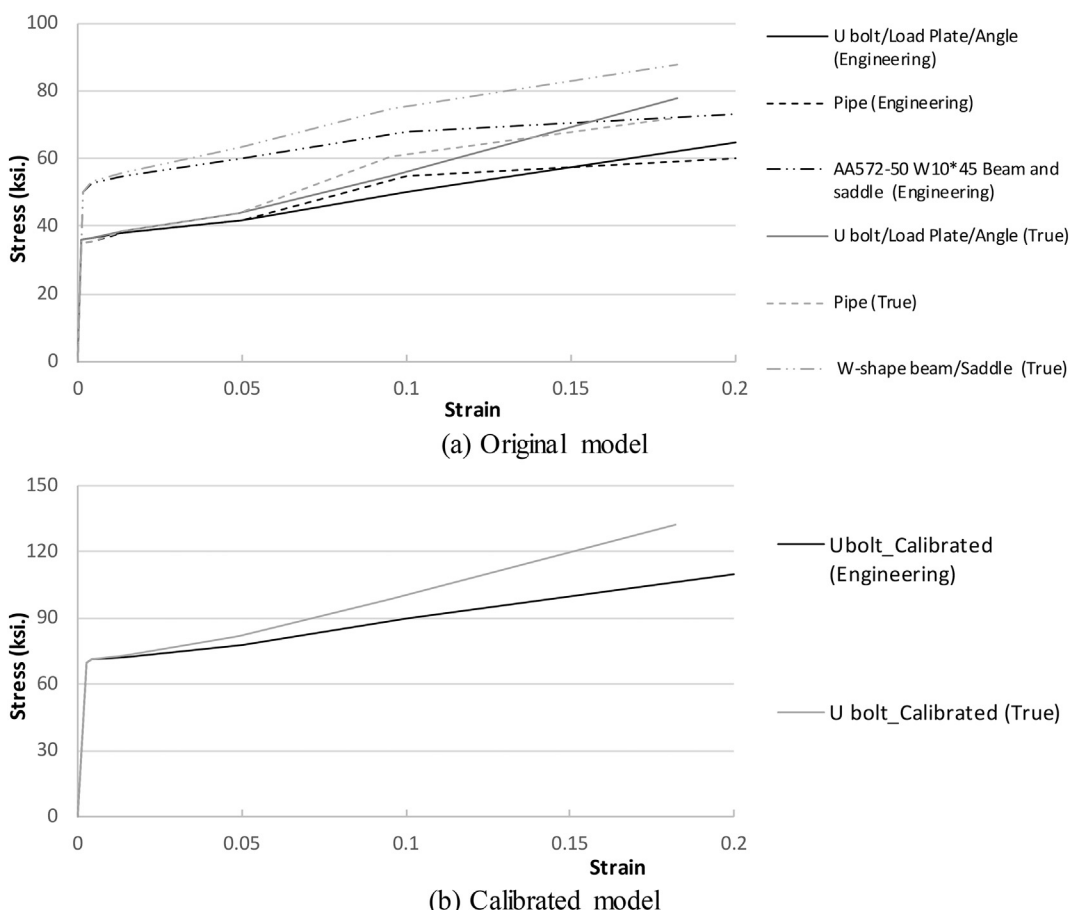
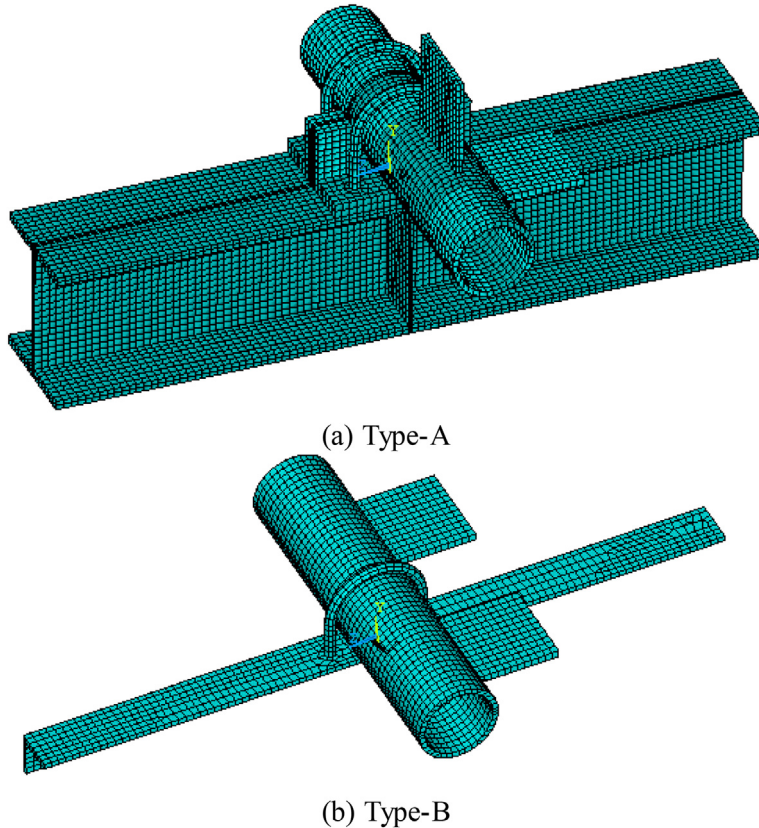


Fig. 10. Engineering and true stress-strain data.



**Fig. 11.** FEM of Type-A specimen.

Surface contact element pairs Conta173/Targe170 were used to model the interaction between the U-bolt and pipe, saddle and pipe, saddle and beam, nuts and beam, shank and sides of the saddle, and top flange of the W-shaped beam. On the Type-A specimen, one layer thin rubber was placed between the saddle and the base beam. The rubber was not included into the mode and the friction coefficient for between the saddle and the base beam was calibrated on the model as 0.75. For the friction coefficient at the other location with steel-to-steel contact, a literature review indicated that a wide range from 0.1 to 0.3 has been commonly used (Ju et al. 2005 and [8]). On this model, the friction coefficient for the steel-to-steel contact was calibrated as 0.2. Zero cohesion was defined for all the contact interaction. Since the W-shaped beam was tied-down on the ground with high pressure during the test (see Fig. 3) and resulted in high friction resistance between the bottom flange of the W-shaped beam and the ground, the bottom flange of the W-shaped beam was fixed on the FEM. The preload was applied onto the nut/washer elements in the same way as that used by McCarthy and McCarthy [6] and McCarthy et al. [7] that assigning a thermal expansion coefficient, and continually increasing the temperature on the nut/washer element until the strain at each gage location showed reasonable consistency with the experimental data. And the horizontal/vertical loads were applied on the plate (welded on the pipe) gradually, until failure. Fig. 11 shows the model geometry and the mesh for both Type-A and Type-B specimens.

The model was first analyzed with the standard material properties of  $f_y = 36$  ksi and  $f_u = 60$  ksi for A36 steel. However, the analytical results showed a difference when compared to the experimental results. Fig. 7-b compares the force vs. displacement curves on the Type-A specimen subject to the vertical load. It is apparent that the experimental results indicated a system yield point at about 18 kips, but the FEM results showed a system yield point when load was about 10 kips. Table 3 compares the ultimate capacities between the analytical and experimental

results. For the Type-A specimen subjected to the vertical loading and the Type-B specimen under horizontal loading, the failure on the tested specimens occurred in the thread region at the thin cross-section (with an area of about  $0.31 \text{ in}^2$ ), while the FEM did not include the thread and had a consistent cross-section area of about  $0.44 \text{ in}^2$ . To account for the thin cross-section at the thread region, failure was identified when stress at the thread achieved a ratio of  $0.31 \div 0.44 \times f_u$ . The corresponding strain was used to find the failure loading. For the two Type-A specimens and the Type-B specimen, the FEM resulted in an ultimate capacity of 38% to 47% lower than the test results. This difference was considered induced by the inaccuracy of the material property of the U-bolt in the FE model. This is because the U-bolt is made by bending a straight steel rod over 90 degree. The large deformation on the shanks induced a significant change in the stress-strain curve. Because of this, the stress-strain curve for the U-bolt was calibrated with  $f_y = 70$  ksi and  $f_u = 110$  ksi as shown in Fig. 10. Table 3 compares the ultimate capacities from the calibrated model against the experimental results for each test. The two Type-A specimens and the Type-B specimen show a small difference of 2% to 8%. Fig. 12-a shows the von Mises strain distribution on the U-bolt after preload. The maximum strain after

**Table 3**  
Ultimate capacity comparisons.

Specimen	Loading	Test Result	Original FEM		Calibrated FEM	
			Ultimate Capacity	Ultimate Capacity	Difference	Ultimate Capacity
Type-A	Horizontal	38 kips	20 kips	47%	36 kips	5%
Type-A	Vertical	24 kips	15 kips	38%	26 kips	8%
Type-B	Horizontal	35 kips	20 kips	42%	34 kips	2%

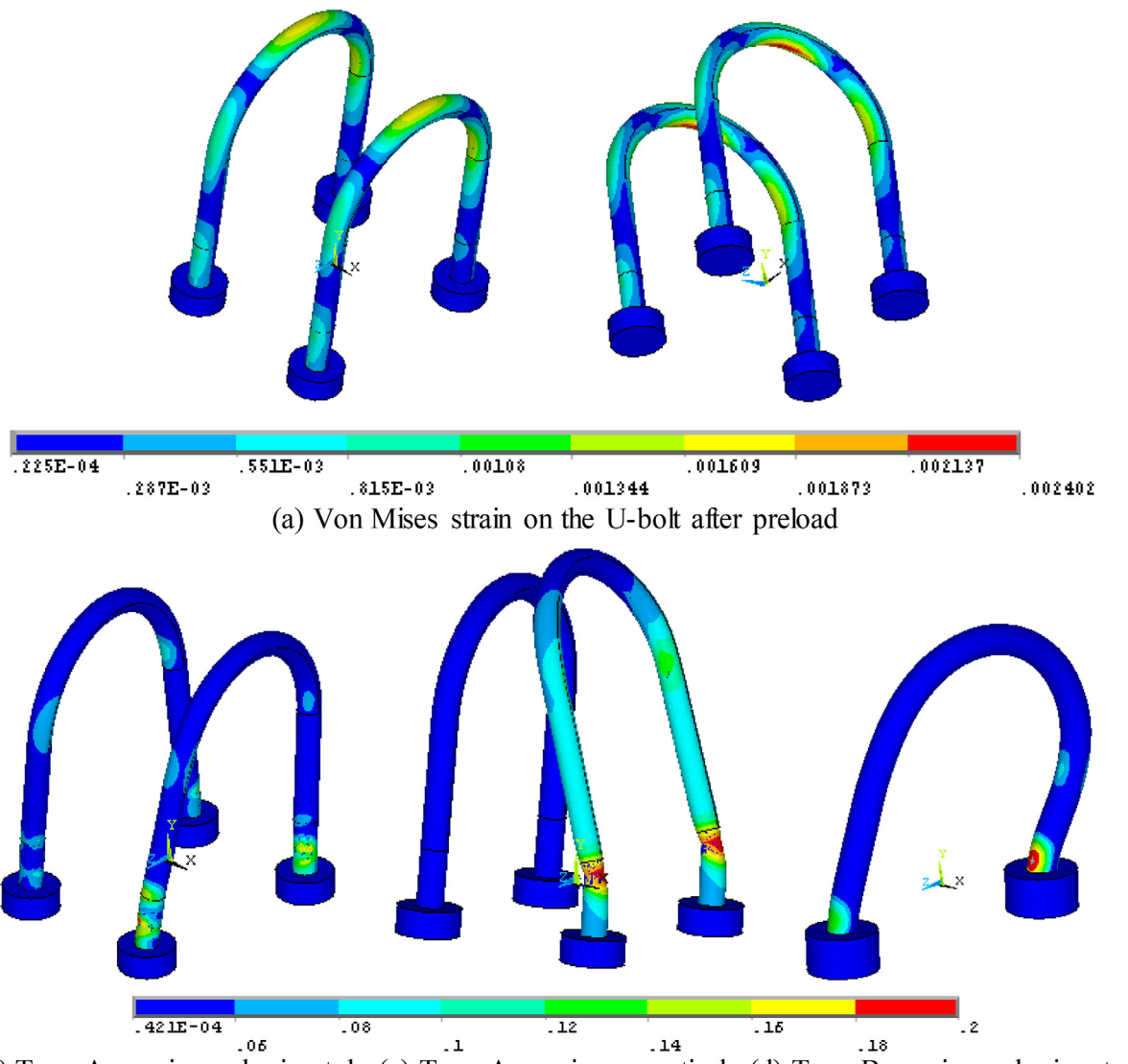


Fig. 12. von Mises strain on the U-bolt at ultimate stage.

preload occurs at the interface between the U-bolt and pipe with a stress concentration resulting in a strain of about 0.0024. Fig. 12-b to -d shows the von Mises strain distribution on the U-bolt at the ultimate stage with an exaggerated deformed shape. Although Fig. 12-b shows

the maximum strain occurs at the shank (above the thread region), a detailed observation indicates that the thread region (blocked by the nuts) achieved a stress equal to  $0.31 \div 0.44 \times f_u$  before the shank reached yielding. Figs. 5 to 9 compare the experimental results to the

**Table 4**  
Materials of interest.

Steel Grade		Diameter (in.)	Yield Strength (ksi)	Ultimate Strength (ksi)
Stainless Steel	ASTM A320, Class 1, Grade B8/B8A	All	30	75
	ASTM A320, Class 2, Grade B8	3/4 and under	100	125
	ASTM F593, Group 1, Alloy 304/304L	Condition A	30	75
		Condition CW2	45	85
	ASTM F593, Group 2, Alloy 316/316L	Condition A	30	75
		Condition CW2	45	85
	ASTM F593, Group 3, Alloy 321/347	Condition A	30	75
		Condition CW2	45	85
Galvanized Steel	ASTM A499, Type 1	1/2 to 1	92	120
	ASTM A307, Grade B	1/4 to 4	Not given	60
	ASTM F1554, Grade 36	1/4 to 4	36	58
	ASTM F1554, Grade 55	1/4 to 4	55	75

\* Initial Young's Modulus of 29,000 ksi for all.

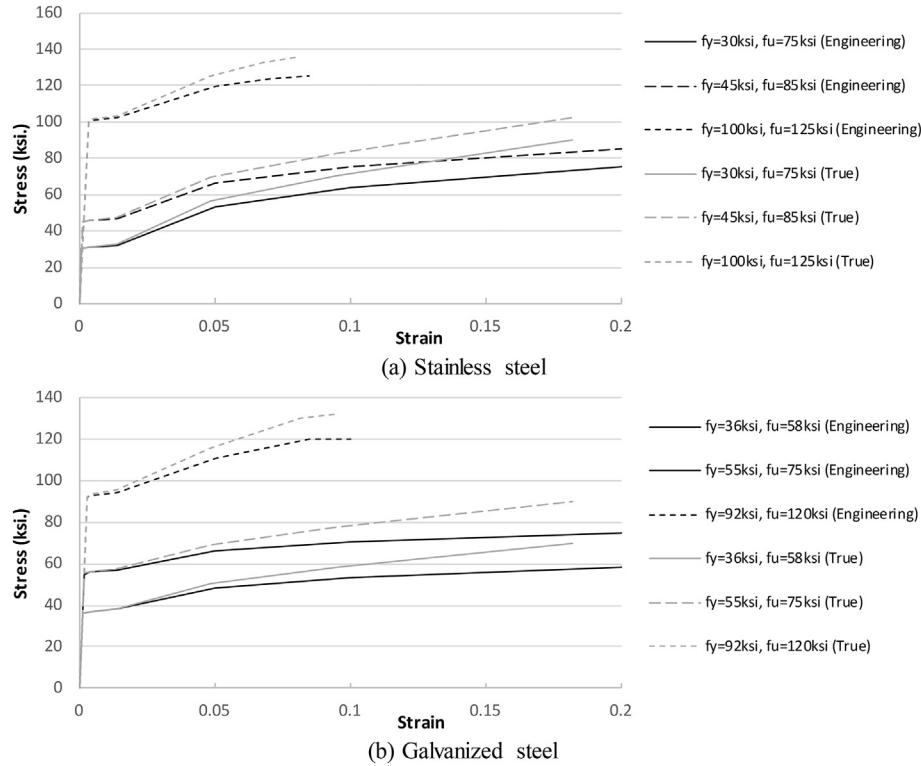


**Fig. 13.** Stress-strain curves of the materials studied during parametric study.

analytical results (before yielding) from the calibrated models with  $f_y = 70$  ksi and  $f_u = 110$  ksi for all three specimens. In general, the analytical results showed good agreement with the experimental results and the modeling approach appears valid for the parametric study.

#### 4. Parametric study

The parametric study was performed to understand the behavior of the U-bolt connections with different material properties and subject to various loading conditions. Given that the laboratory tests on the specimens were conducted and the model calibration was performed based on the most frequently used 3/4-in. diameter U-bolt, the parametric study was also performed for the 3/4-in. diameter U-bolt connection. According to the Iowa DOT Standard Specifications for Highway and

Bridge Construction [2] Article 4187.01, C, 2, both galvanized steel U-bolts of various grades and stainless steel U-bolts of various grades are allowed for the U-bolt connections. Table 4 lists all of the types of steel that are allowed for the 3/4-in. diameter U-bolt. During the parametric study, all of the steel grades highlighted in yellow in Table 4 were studied. The ASTM A307, Grade B ( $f_u = 60$  ksi) galvanized steel, whose yield strength is not defined, was not studied. The effects of these material properties were studied by modifying the constitutive models of the materials in the FEM, while the geometric properties of the FEM were kept the same. Fig. 13 plots the stress-strain curves for each type of material that was studied during the parametric study. The true stress-strain curve was converted based on the engineering stress-strain (shown in Fig. 13), which was established with an initial Young's

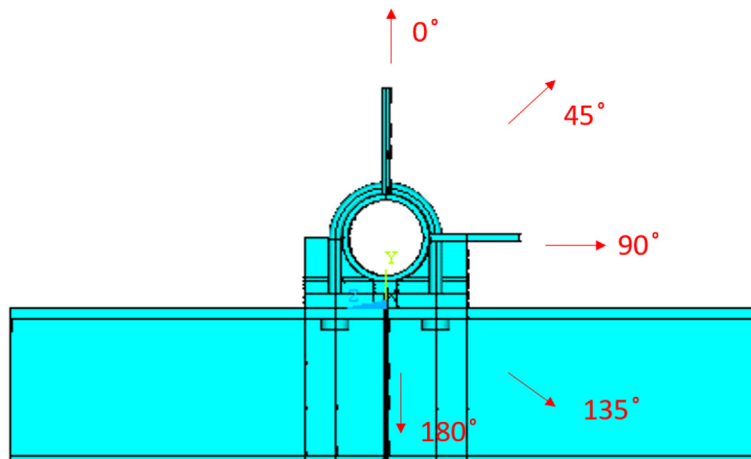
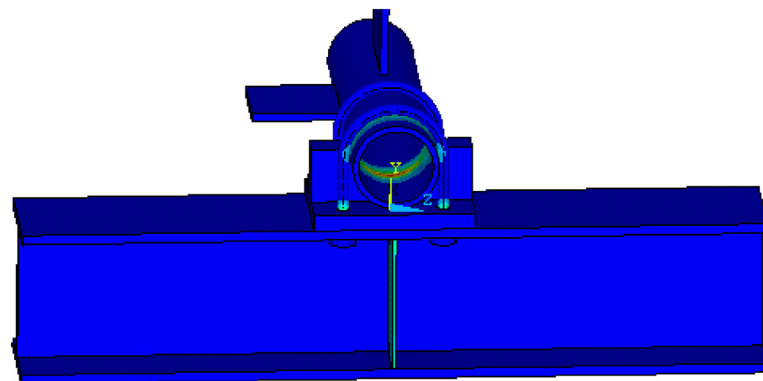


**Fig. 14.** Parametric study loading directions relative to the vertical direction for the Type-A specimens.

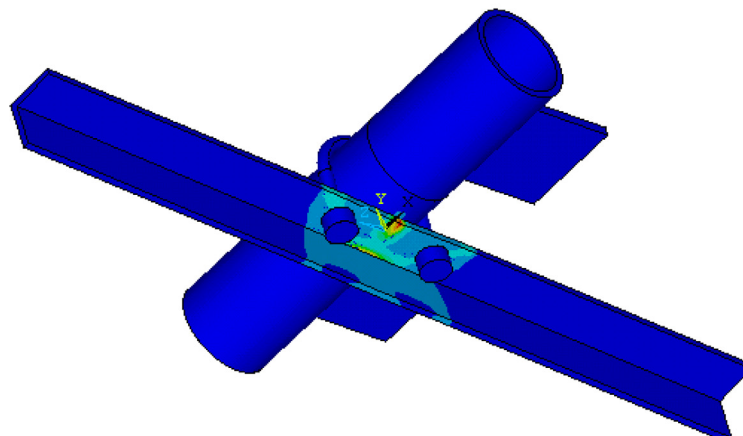
**Table 5**

Parametric study results.

Material Type		Stage of Interest	Type-A Specimen					Type-B Specimen					
			0°	45°	90°	135°	180°	0°	45°	90°	135°	180°	
Stainless Steel	$f_y = 30 \text{ ksi}$ $f_u = 75 \text{ ksi}$	Yield	Capacity (kips)	<1	<1	<1	<1	8.5	1	1.5	1.5	3	
		Location	Thread	Thread	Shank	Thread	Thread	Thread	Thread	Thread	Thread	Angle	
	$f_y = 45 \text{ ksi}$ $f_u = 85 \text{ ksi}$	Ultimate	Capacity (kips)	18	15	24	19	23	41	12	29	17	
		Location	Thread	Thread	Shank	Thread	Thread	Thread	Thread	Thread	Thread	Angle	
	$f_y = 100 \text{ ksi}$ $f_u = 125 \text{ ksi}$	Yield	Capacity (kips)	1	<1	1	<1	2	11.5	2	2.5	2	3
		Location	Thread	Thread	Shank	Thread	Thread	Thread	Thread	Thread	Thread	Angle	
	$f_y = 36 \text{ ksi}$ $f_u = 58 \text{ ksi}$	Ultimate	Capacity (kips)	20	17	27	22	24	48	12	30	19	14
		Location	Thread	Thread	Shank	Thread	Pipe	Thread	Thread	Thread	Angle	Angle	
	$f_y = 55 \text{ ksi}$ $f_u = 75 \text{ ksi}$	Yield	Capacity (kips)	6	2.5	5.5	4	9	23	5	7	6.5	3
		Location	Thread	Thread	Shank	Thread	Thread	Thread	Thread	Thread	Thread	Angle	
	$f_y = 92 \text{ ksi}$ $f_u = 120 \text{ ksi}$	Ultimate	Capacity (kips)	30	25	40	32	24	48	16	45	19	14
		Location	Thread	Thread	Shank	Pipe	Pipe	Thread	Thread	Thread	Angle	Angle	



(a) Type-A



(b) Type-B

**Fig. 15.** Critical location at the angle.

modulus of 29,000 ksi and a peak strength strain of 0.2 ( $f_u < 100$  ksi) and 0.1 ( $f_u > 100$  ksi).

Additionally, the orientation of the loading relative to the beam was studied analytically to understand the behaviors of the specimens under those loading conditions. Fig. 14 shows the loading directions relative to the vertical direction for the Type-A specimens. The Type-B specimen used the same method to designate the loading directions. During the parametric study, one FEM was developed for each specimen type with a certain material property and loading direction, and analyzed with the nonlinear material and geometric properties. In total, 60 analyses were performed. Similar to the calibrated model, a preload was applied to the model until the U-bolt achieved a strain similar to that measured during testing. Then, the model was gradually loaded until failure occurred. To find the location that first achieved the yield or ultimate strain, small load steps were used in the analysis, and the results from each load step were carefully observed at the critical locations including U-bolt shank, thread, pipe, and angle. The yield or ultimate stage was identified when the strain at the critical location initially achieved the value corresponding to the yield or ultimate strength. Note that the yield or ultimate strengths at the thread region were reduced by a ratio of 0.31 ÷ 0.44 to account for the thin cross-section at the thread region on the actual specimen.

To gain an understanding of the structural behavior of both U-bolt connection types, both yield capacity and ultimate capacity results were output and are listed in Table 5. The critical locations are shown previously in Fig. 12-a and -b at the shank and thread for the Type-A model and in Fig. 12-c at the thread for the Type-B model. Fig. 15 show the critical location (red) at the pipe and angle respectively. Note that, for the Type-B model subject to 180° loading, the load was carried by the angle without inducing any stress on the U-bolt. The results in Table 5 show a relatively low yield capacity but high ultimate capacity, which indicates a good ductility before reaching failure. It also could be concluded that the thread region is the most vulnerable location, as most of the failures start in that region. In addition, it should be noticed that the results in Table 5 could be used with the following limitations:

- The capacities presented are only for the 3/4-in. diameter U-bolt on the specific connection structure (Type-A or Type-B) with certain materials. The capacity of the other size U-bolt with different connection details and material type should be determined from further research and should not be estimated from the information in Table 5.
- The laboratory tests were performed with loading directions of only 0° and 90° for Type-A specimens and 90° for the Type-B specimen. The results for other loading directions were obtained from the analytical study.
- The capacities were calculated on a system basis, not just the U-bolt. For example, under certain conditions, the Type-B system first yielded or achieved the ultimate strength on the pipe or angle, not the U-bolt. The replacement of accessory parts, such as the angle or pipe, may change the system capacity.

## 5. Conclusions

A comprehensive literature search on the utilization of and modeling of U-bolt connections was conducted for this research project. Three laboratory tests were conducted on two types of specimens. The data collected from the tests were analyzed and then used to calibrate various FEMs. The calibrated models were then used in the parametric study to calculate the yield and ultimate capacities of both specimen types with various material properties and load directions. A few conclusions can be summarized from different phases of this work as follows:

- Not many research investigations on the capacity of U-bolt connection have been conducted in the field of civil engineering. In addition, most manufacturers of U-bolts do not intend for them to be used in the ways currently detailed.
- The results from both laboratory tests and analytical solutions indicate that different failure modes occur when the loading is in different directions.
- The results from the analytical study show a relatively low yield capacity, but indicate that the details have good ductility before reaching failure.
- The parametric study results indicate that the thread region is the most vulnerable location and that most of the failures start from that region.

The research summarized in this report represents a major step toward developing a better understanding of the behavior and design of U-bolt connections. However, several questions remain that could be answered by conducting additional research, as follows:

- Additional laboratory tests should be performed on high-strength U-bolts with loading directions of 135° and 180°, because the failure locations predicted by the FEM analyses with high-strength U-bolts are different from those captured in the laboratory tests.
- Given that almost all of the material types appear to have low yield capacity, the fatigue performance of the U-bolt connection should be investigated to understand the impact of repeated loads near the yield load. Additional laboratory tests are recommended to study the fatigue performance of the U-bolt connections.
- Given that both experimental and analytical work were conducted on the 3/4-in. diameter U-bolt, further research is recommended on U-bolt connections with other sizes to obtain the relationship between the U-bolt size and connection capacity.

## Declaration of Competing Interest

The authors declare that they have no known competing financial interests or personal relationships that could have appeared to influence the work reported in this paper.

## References

- [1] A.T. Diamantoudis, C.A. Apostolopoulos, Body mounting and ADR requirement for tank vehicles carrying dangerous goods, *Tech. Chron. Sci. J.* 4 (1–2) (2002) 19–27 in Greek with extended summary in English.
- [2] Iowa DOT, Standard Specifications for Highway and Bridge Construction, Article 4187.01, C, 2 (with last revised 4/16/2019 at <https://www.iowadot.gov/erl/current/GS/content/4187.htm> 2020).
- [3] S.-H. Ju, C.-Y. Fan, G.H. Wu, Three-dimensional finite elements of steel bolted connections, *Eng. Struct.* 26 (3) (2004) 403–413.
- [4] J. Kim, J.-C. Yoon, B.-S. Kang, Finite element analysis and modeling of structure with bolted joints, *Appl. Math. Model.* 31 (5) (2007) 895–911.
- [5] D. Kirby, R. Charniga, A finite element and experimental analysis of a light truck leaf spring system subjected to pre-tension and twist loads, Technical Paper No. 2005-01-3568 2005 SAE Commercial Vehicle Engineering Conference, November, Chicago, IL, 2005.
- [6] C.T. McCarthy, M.A. McCarthy, Three-dimensional finite element analysis of single-bolt, single-lap composite bolted joints: part II—effects of bolt-hole clearance, *Compos. Struct.* 71 (2) (2005) 159–175.
- [7] M.A. McCarthy, C.T. McCarthy, V.P. Lawlor, W.F. Stanley, Three-dimensional finite element analysis of single-bolt, single-lap composite bolted joints: part I—model development and validation, *Compos. Struct.* 71 (2) (2005) 140–158.
- [8] M.K. Shetty, Development of a Lead Spring U-Bolt Load Transducer: Part of an On-board Weighing System for Off-Highway Log Trucks, MS thesis University of British Columbia, Vancouver, 2006.